Nanoscale

Vertical van der Waals Heterojunction Diodes comprising 2D Semiconductors on 3D β-Ga2O3

Journal:	*Nanoscale*
Manuscript ID	NR-ART-04-2023-001987
Article Type:	Paper
Date Submitted by the Author:	28-Apr-2023
Complete List of Authors:	Leblanc, Chloe; University of Pennsylvania, Electrical and Systems Engineering Mudiyanselage, Dinusha; Arizona State University, Song, Seunguk; University of Pennsylvania, Electrical and Systems Engineering Zhang, Huairuo; NIST, MML Davydov, Albert; NIST Fu, Houqiang; Arizona State University Jariwala, Deep; University of Pennsylvania, Electrical and Systems Engineering

Vertical van der Waals Heterojunction Diodes comprising 2D Semiconductors on 3D β-Ga_2O_3

Chloe Leblanc,[a] Dinusha H. Mudiyanselage,[b] Seunguk Song,[a] Huairuo Zhang,[c,d] Albert V. Davydov,[c] Houqiang Fu[b] and Deep Jariwala[a]

[a.] *Department of Electrical and Systems Engineering, University of Pennsylvania, Philadelphia, PA 19104, USA.*

[b.] *School of Electrical, Computer, and Energy Engineering, Arizona State University, Tempe, AZ 85287, USA.*

[c.] *Materials Science and Engineering Division, National Institute of Standards and Technology (NIST), Gaithersburg, MD 20899, USA.*

[d.] *Theiss Research, Inc., La Jolla, CA 92037, USA.*

e-mail: dmj@seas.upenn.edu

Abstract: Wide bandgap semiconductors such as gallium oxide (Ga_2O_3) have attracted much attention for their use in next-generation high-power electronics. Although single-crystal Ga_2O_3 substrates can be routinely grown from melt along various orientations, the influence of such orientations has been seldom reported. Further, making rectifying p-n diodes from Ga_2O_3 has been difficult due to lack of p-type doping. In this study, we fabricated and optimized 2D/3D vertical diodes on β-Ga_2O_3 by varying the following three factors: substrate planar orientation, choice of 2D material and metal contacts. The quality of our devices was validated using high-temperature dependent measurements, atomic-force microscopy (AFM) techniques and technology computer-aided design (TCAD) simulations. Our findings suggest that 2D/3D β-Ga_2O_3 vertical heterojunctions are optimized by substrate planar orientation (-201), combined with 2D WS_2 exfoliated layers and Ti contacts, and show record rectification ratios (> 10^6) concurrently with ON-Current density (> 10^3 A cm^{-2}) for application in power rectifiers.

Introduction

Gallium oxide (Ga_2O_3) is a promising candidate for high-power and high-temperature electronic devices and UV-range optical devices. Its properties include a high critical electric field of 8 MV cm^{-1}, an electron saturation velocity up to 2x10^7 cm s^{-1} and an easily swayed n-type conductivity with a bandgap of 4.9 eV[1]. More importantly, it can outperform other wide bandgap materials like GaN or SiC in power electronics devices[2,3]. From an industrial standpoint, Ga_2O_3 native substrates are of particular interest as their melt-grown bulk single crystal fabrication techniques are very affordable at the large production scale[4]. Monocyclic (β-phase) Ga_2O_3 is the crystal's most stable polymorph and has already been demonstrated in MOSFETs and UV transparent optoelectronic devices[1,5,6]. Its transmissivity >80% in the visible range eliminates the need for optical filters and bandgap tuning through alloying[7]. Heterointerfaces between 3D substrates such as Ga_2O_3 and 2D materials are appealing as they merge the complementary properties of self-passivation in 2D with precise doping schemes in 3D materials[11]. The success of graphene has paved the way for the assimilation of 2D transition-metal dichalcogenides (TMDCs) into next-generation nanoelectronics. Their self-passivated surfaces and sizable bandgaps enable high-quality, defect-free heterogeneous integration and superior electrostatic control[8,9,10].

In this study, we fabricated 2D/3D β-Ga_2O_3 vertical heterojunctions and comprehensively assessed the effect of the choice of 2D material, contact metal and β-Ga_2O_3 crystalline orientation on their performance. The highly anisotropic properties of β-Ga_2O_3 have been theoretically predicted and reported in numerous studies[12,13,14,15,16]. Their influence on subsequent device performance was therefore a point of focus, with three orientations of degenerately n-doped β-Ga_2O_3 considered: (001), (010) and (-201). Tungsten diselenide (WSe_2), tungsten disulfide (WS_2) and black phosphorus (BP) were studied as potential junction-forming 2D semiconductor p-type materials (Figure S1). WS_2 and WSe_2 are well-established TMDCs that share a trilayer, van der Waals-bonded S/Se-W-S/Se structure[17]. Their properties have already been incorporated in high-performing optoelectronic devices, field-effect transistors (FETs) and light-emitting diodes (LEDs) and other heterostructures[18,19,20,21]. Although WS_2 and WSe_2 are similar in structure, their bandgaps and hence band alignments are slightly different: WSe_2 presents a type 2 band alignment with Ga_2O_3, whereas WS_2 yields a type 1 alignment, as represented in Figure S1. Comparing WSe_2/Ga_2O_3 and WS_2/Ga_2O_3 heterostructures allowed us to observe the contrast in performance resulting from carriers along the TMDC conduction band reaching either a potential barrier or well. BP is a stable allotrope of phosphorus that has displayed carrier mobilities of up to 1000 cm^2 $V^{-1}s^{-1}$ and 10^5 on/off current ratios, thereby overshadowing the electrical properties of TMDCs[22,23,24]. Unlike WS_2 and WSe_2, it also maintains a widely tunable direct bandgap which ranges between 0.3 eV (bulk) and 2.1 eV (monolayer)[25]. In 2D semiconductor devices, a crucial and ongoing subject of many studies has been

minimizing the voltage drop at the semiconductor-metal junction, which is why we decided to compare electron beam (E-beam) evaporated titanium (Ti), molybdenum trioxide (MoO_3) or palladium (Pd) as candidates for contact metals, with thicknesses based on previous reports of low-resistance: Ti/Au (10/90nm), MoOx/Au (3/30nm), Pd/Au (30/70nm)[26,27,28].

The structure and properties of our devices were evaluated using current-voltage (I-V) measurements at varying temperatures, atomic-force microscopy (AFM) techniques and technology computer-aided design (TCAD) simulations. Our findings suggest that 2D/3D β-Ga_2O_3 vertical heterojunctions are optimized by planar orientation (-201), combined with 2D WS_2 and Ti contacts.

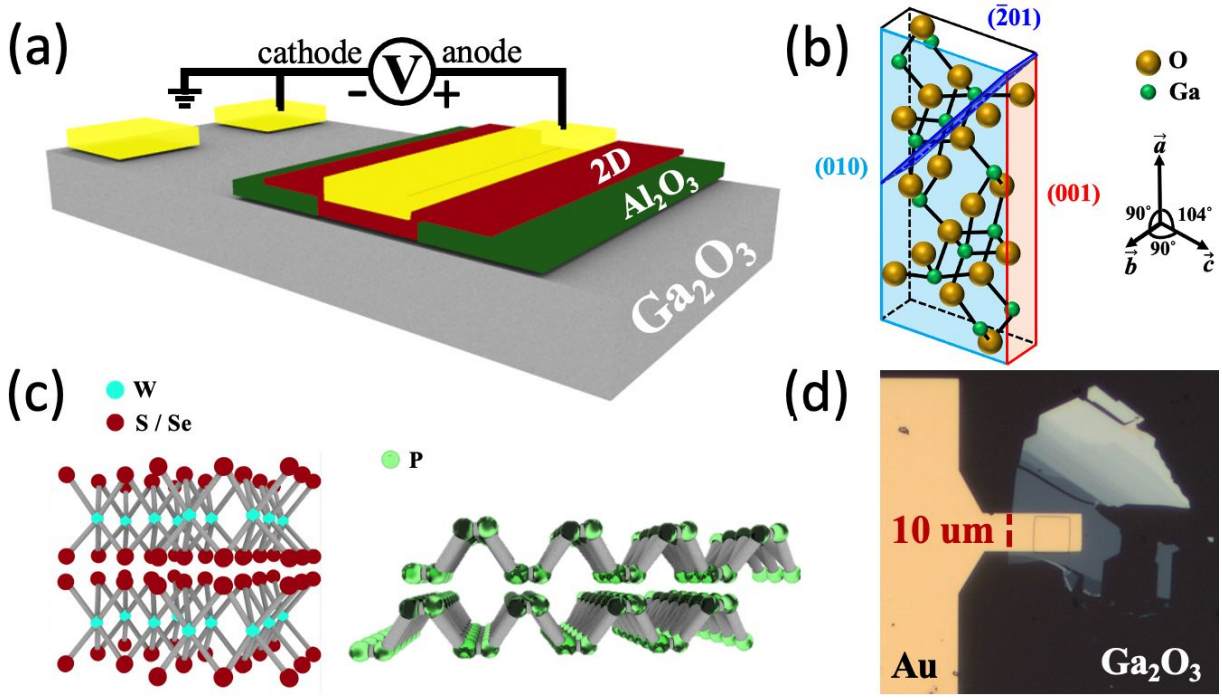

Fig. 1 (a) Schematic layout of the heterostructure. The Ga_2O_3 substrate is represented in gray, the Al_2O_3 layer in green, the 2D material in red and the metallic electrodes (i.e. Ti/Au, Pd/Au or MoO_3/Au) in yellow. (b) Model representation of the different Ga_2O_3 planes. (c) Two layers of repeated unit cells of the 2D materials. Leftmost is the TMDC: center blue atoms are W and red atoms, either Se or S. Rightmost structure is the BP, with P atoms modeled in green. (d) Optical micrograph of a representative 2D/3D heterostructure diode device.

Results and Discussion

We fabricated heterojunctions using single-crystalline β-Ga_2O_3 single crystals of varying orientations: (-201), (010), (001) and mechanically exfoliated van der Waals (vdW) 2D crystals of WS_2, WSe_2, and BP from commercially purchased bulk 2D crystals. We used standard thin-film deposition electron-beam lithography, wet-etching and physical vapor deposition techniques to fabricate the devices. Our heterojunctions followed the design/structure shown in Fig. 1(a) and the measurements were carried out as described in the *Methods* section. Annular dark-field scanning transmission electron microscopy (ADF-STEM) and bright-field (BF) STEM imaging of a WSe_2 junction with MoO_3/Au contacts on a (010)-oriented Ga_2O_3 substrate (Fig. 2, Fig. S2) show sharp interfaces between the metal/2D/3D heterojunction materials. To control the junction area, we deposited a lithographically defined insulating Al_2O_3 layer that outlined the device dimensions. Topography and phase imaging (Fig. S3) clearly show the depression below the top electrode where the heterojunction forms.

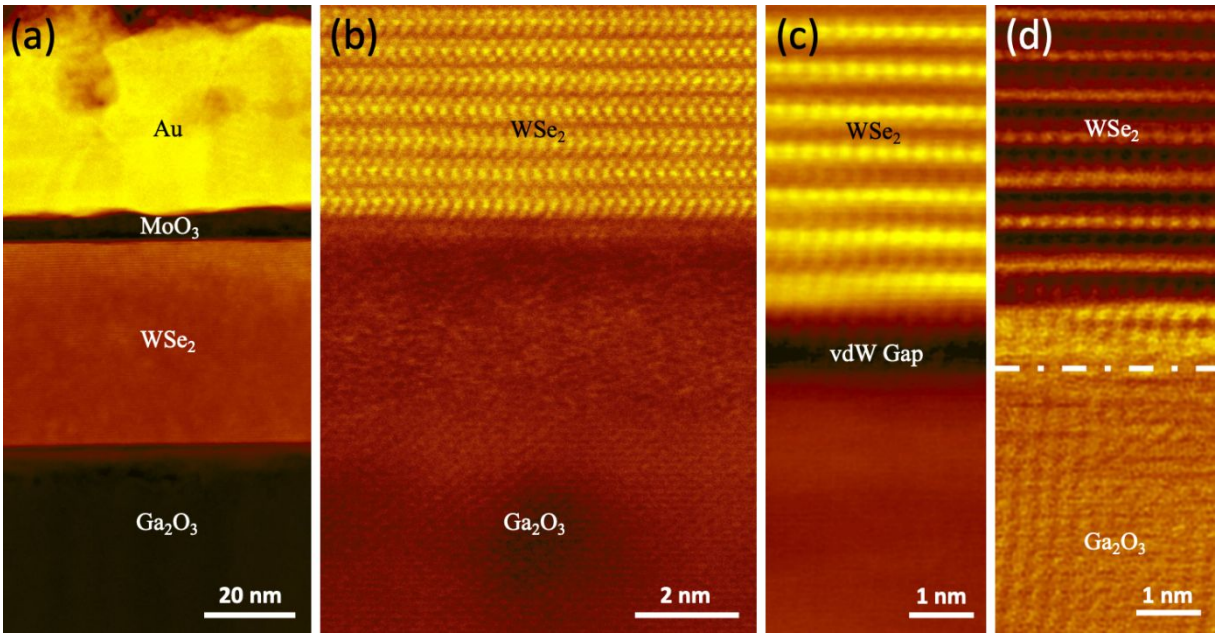

Fig. 2 Characterization of WSe_2 junction cross-sections on (010)-oriented Ga_2O_3 with MoO_3/Au contacts. (a) Low magnification ADF-STEM image showing the structure layers of the device. (b) Atomic resolution ADF-STEM image. The WSe_2/ Ga_2O_3 interface layer was subjected to FIB ion-beam damage. (c) ADF-STEM and corresponding BF-STEM (d) Images taken from a thick sample area showing the van der Waals (vdW) gap at the WSe_2/ Ga_2O_3 interface. ADF-STEM characterization of a WS_2/ (010) Ga_2O_3 junction are available in supplementary information.

The reverse and low forward bias regions in Fig.3 present current densities that are both very low (<10^{-10} A μm^{-2}) and independent of the applied voltage. These could therefore be attributed to leakage and the recombination-generation current (R-G) that usually dominates these regimes of operation[31]. The turn-on voltages V_{ON} of the junctions presented in Fig.3 varied between approximately 0.25V and 1V—a range that encompasses the turn-on voltages of multiple previously reported β-Ga_2O_3 substrate devices[32,33]. We attribute these non-zero V_{ON} values to the presence of an electron barrier accumulated at the junction active area, causing an aperture choke and potential barrier to build up[34]. For applied biases greater than V_{ON} and before the junctions reach saturation, the exponential current density increase for low changes in applied bias matches the strongly rectifying property of ideal diodes in the linear regime, where the devices are driven by the diffusion current across the internal 2D/3D potential barrier[31]. TCAD simulations were able to accurately mimic the (-201) β-Ga_2O_3 behavior, as this orientation yields excellent electrical properties and the smallest deviations from ideal behavior compared to other planes (Fig.3(a)). The current density caused by thermionic emission abides to the formula[35]

$$J = J_s\left(exp\left(\frac{qV}{nkT}\right) - 1\right)$$

where

$$J_s = q\left(\frac{D_{n2}n_{i2}^2}{L_{n2}N_{a2}} + \frac{D_{p1}n_{i1}^2}{L_{p1}N_{d1}}\right)$$

, where J_s is the saturation current density, k is the Boltzmann constant, T is the temperature in Kelvin, N_{d1} and N_{a2} are the electron and hole concentrations, in β-Ga_2O_3 and 2D material at equilibrium, D_{n2} (D_{p1}) and L_{n2} (L_{p1}) are the diffusion constant and diffusion length for electrons (holes) in β-Ga_2O_3 (2D material), V is the external applied voltage, and n the ideality factor. Ideality is often used in assessing diode performance, where n nearing unity signals an ideal behavior, where drift-diffusion current is dominant. Our lowest extracted n values are listed along with their standard deviations in Table 1. We hypothesize that the device-to-device variation occurs due to difference in 2D crystal quality from flake to flake as they are derived from mechanical exfoliation as well as variation in interface quality from device to device as the heterojunctions are made discretely via a stamp transfer process and the 3D material is prone to surface roughness. This can introduce parasitic resistance, which along with interface states can cause a recombination current component during forward bias to occur, resulting in an alteration of the ideality factor of the devices. An ideality n >2 indicates a recombination of holes and electrons occurs at the heterojunction and deviates from the ideal drift-diffusion model. We observed that β-Ga_2O_3 samples with orientation (-201) yield the best performing diodes. The lowest ideality factors along that orientation were 1.18 (BP & Ti/Au contacts), 1.22 (WS_2 & Ti/Au contacts) and 1.43 (WS_2 & Pd/Au contacts) in line with some of the best 2D/3D van der Waals heterojunction diodes reported in the past.[36,37,38]

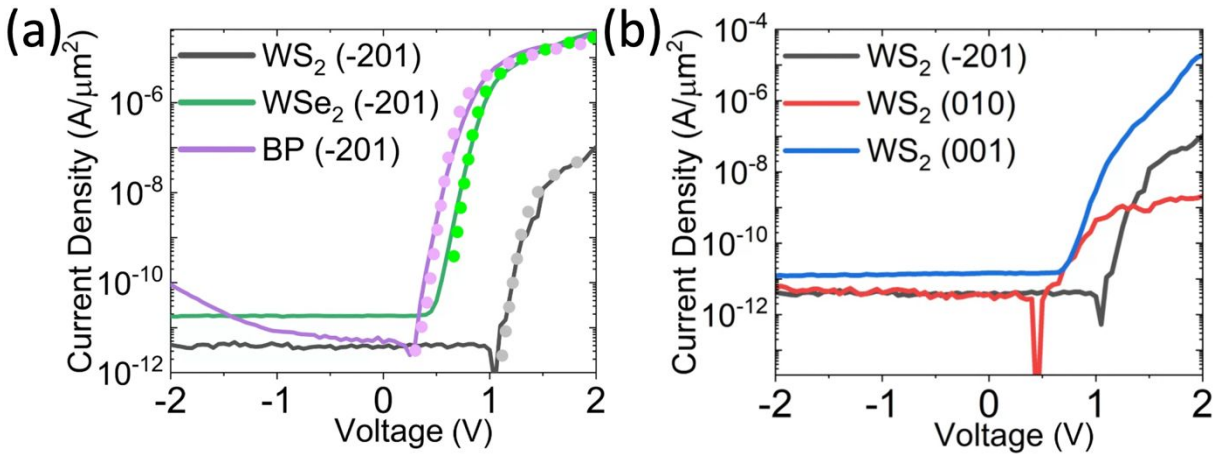

Fig. 3 Current density vs. voltage graph of the lowest recorded ideality factors for the (-201) Ga_2O_3 orientation (a) and WS_2 2D material (b). Dotted lines represent the predicted behaviors from the TCAD simulations.

Crystal Orientation (Top surface)	2D Semiconductor		
	WSe_2	WS_2	BP
(001)	1.20	2.39	1.88
(010)	2.79	1.60	1.68
(-201)	1.49	1.22	1.18
Simulated (-201)	1.36	1.05	1.11
Standard deviation (-201)	0.661	1.36	0.239

Table 1 Lowest recorded ideality factors, simulated ideality factors and standard deviation by 2D material and crystal orientation, across all contact types.

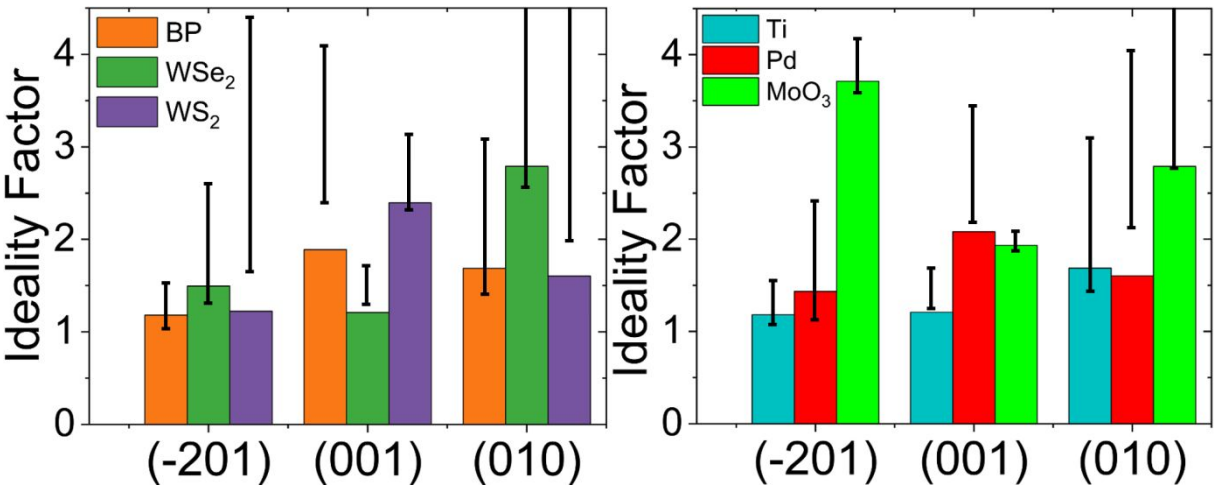

Fig. 4. Bar chart of the lowest recorded ideality factors and the standard deviations by 2D material (left) and contact metal (right). The standard deviations are centered around the average ideality values of each category.

Acoustic phonons and ionized impurities are commonly considered as the most significant sources of carrier scattering inside a crystal lattice. These are attributed to lattice vibrations in the material, which inevitably occur above 0 K. A higher atomic density in the lattice therefore leads to more scattering and a lower carrier mobility. In monocyclic crystals, the interplanar spacing can be calculated as

$$d = \sqrt{\frac{1}{a^2} - \frac{h^2}{sin^2\beta} + \frac{k^2}{b^2} + \frac{l^2}{c^2 sin^2\beta} - \frac{2hl\,cos\beta}{ac\,sin^2\beta}}$$

, where h, k and l are the Miller indices along the x, y, and z axes respectively. Taking the intrinsic β-Ga_2O_3 lattice constants to be **a**=12.21 Å, **b**=3.04 Å, **c**=5.80 Å and **β**=103.8°, we find the distances d_{001} = 2.55 Å, d_{010} = 3.04 Å and d_{-201} = 4.68 Å for the crystalline orientations (001), (010) and (-201) respectively[39]. These imply that the (-201) plane experiences much fewer lattice collisions as its planes are further apart. Moreover, the electric conductivity in bulk β-Ga_2O_3 differs along crystal axes **a**, **b** and **c**[40]. Subsequently, current conduction should be altered by substrate orientation, which in turn will be reflected in the device ideality factors[41]. The (-201) plane also benefits from a higher density of dangling oxygen bonds that promotes the interfaces with 2D materials[42,43]. Dangling bonds also provide carrier trapping, recombination and fermi-level pinning which all contribute to non-idealities in a heterojunction diode.[44,45,46,47]

Bulk β-Ga_2O_3 is also known for its highly anisotropic properties, such as the uneven formation of deep-level defects trickling down from the low crystalline symmetry. Hydrogen for instance has been shown to form complexes with split Ga vacancies most effectively in the (−201) orientation, yielding higher diffusion coefficients in the (010) direction than in the (-201)[48]. Previous studies have reported a β-Ga_2O_3 thermal conductivity approximately three times larger along the (010) direction than along the (100)[13]. Asymmetric phonon modes were also suggested as the cause of significant anisotropic carrier scattering and variations in electron mobility in β-Ga_2O_3 FETs[15]. Recent reports have found an extremely strong Fröhlich interaction in the material, fueled by the high ionicity of the chemical bonds, and the low optical phonon energies[49]. From this they concluded that electron-polar optical phonon (e-PO) interactions must be the dominant intrinsic scattering mechanism in β-Ga_2O_3. This phenomenon exists in bulk GaN, where orientation-dependent scattering rates trickle from the absence of intravalley PO phonon emission along certain directions[50]. In addition, the electrons in the TMDCs may experience random electric fields at the interface with the β-Ga_2O_3[51]. These are time-dependent and can be traced back to Coulomb impurities (CI) at the surface of the substrate and remote interactions with the substrate's surface optical phonons (SO), thereby slowing charge transport in the TMDCs.

A variation in device performance related to the choice of contact metals was also recurrently observed (Fig.4). We found an advantage of Ti/Au over Pd/Au and MoO_3/Au, thereby indicating some degree of contact material-specific resistance. The interfaces could be formed by a van der Waals gap acting as a tunneling barrier for carriers, reducing the charge injection from metals and increasing contact resistance[52]. Our observations also complement the previously reported Ohmic behavior of Ti/Au contacts with the (-201) Ga_2O_3 plane in particular[43]. The same Ti/Au contacts yield Schottky behavior rather than ohmic with the other planes, (001) and (010). We observed the reduction of the ideality factor at increasing temperatures (Fig. S8(a))[53]. At inhomogeneous metal/semiconductor interfaces, regions of highest Schottky barrier height are crossed only if electrons acquire enough momentum, which we provided here by thermal excitation. As a result, the Schottky barrier height increased with temperature. From these measurements we were also able to extract the expected 2D/metal Schottky barrier height (SBH) variation from approximately 0.6 to 0.8 eV in the studied temperature range (Fig. S5(c)). Although it is reasonable to approximate semiclassical thermionic emission as the sole transport mechanism in low SBH values, Fowler-Nordheim (F-N) and direct tunneling are also non-negligible sources of charge transport[8]. Direct tunneling is predominant over Fowler-Nordheim in regions of lower bias, and the inverse is observed at higher biases[54]. F-N tunneling has a linear voltage dependency, whereas direct tunneling shows an exponential dependence[55]. For our studied metal contacts on WSe_2, we found that the crossover between tunneling types occurs at approximately 1.6 V (0.625 V^{-1}). Moreover, these differences in the device electrical properties (Fig.3) are also attributable to the conductivity-modulated hole injection into β-Ga_2O_3. In ultra-wide bandgap materials, conductivity-modulated hole injection is still elusive and needs further investigation. Our 2D/3D devices provide evidence that hole injection into the β-Ga_2O_3 is possible in a similar fashion to p-NiO_x/n-β-Ga_2O_3 heterojunction diodes[56]. Due to the variation of Ga_2O_3 planar orientation, hole injection is altered as reflected in the I-V characteristics.

Kelvin Probe Force Microscopy (KPFM) and Conductive AFM (C-AFM) were performed on the (-201) and (001) β-Ga_2O_3 orientations with WSe_2 for further characterization of the junction's electrical properties and their results compared in figure 5. For junctions of different Ga_2O_3 orientations, the average C-AFM current values dropped off past the outlines of the junctions, as reflected by the sharp decrease in ideality factor values by at least two orders of magnitude (Fig.S6). This confirms the insulating properties of the Al_2O_3 layer. Resistance measurements between the cathode at the edge of the substrate (Fig. 1(a)) and contacts placed directly onto the Al_2O_3 showed no current flow—another proof that the Al_2O_3 layer is properly insulating. The quality of Al_2O_3/β-Ga_2O_3 crystallographic interfaces has also been demonstrated in previous works[29,30]. KPFM measures the surface work-function of a solid by measuring the potential difference between its surface and a sharp tip above[26]. Areas where the potential drop is greater are imaged darker. Our KPFM measurements over both devices revealed a variation in work-function at the surface of the substrate-TMDC interface that matched the alterations in thicknesses of the 2D semiconductor flakes (Fig. 5(c)). This arises from the fact thicker flakes are regions of larger hole

accumulation, resulting in greater Fermi level offsets at the 2D/3D interface (Fig. 5, Table S1). KPFM measurements also indicated the outskirts of our junctions as prone to high hole accumulation. This is due to the topographical drop between the heterojunctions and the Al_2O_3 layers delimiting their area. The depression of the TMDC flake bending into the Al_2O_3 trenches results in the scanning tip detecting a larger vertical accumulation of holes and potential drop. Contrariwise, the KPFM measurements indicate no potential variations in both the uncovered n-type substrate and in the Al_2O_3 areas. This verifies the lack of p-n junction at these locations. A second example of topography, magnitude and KPFM scans is available in Fig.S7.

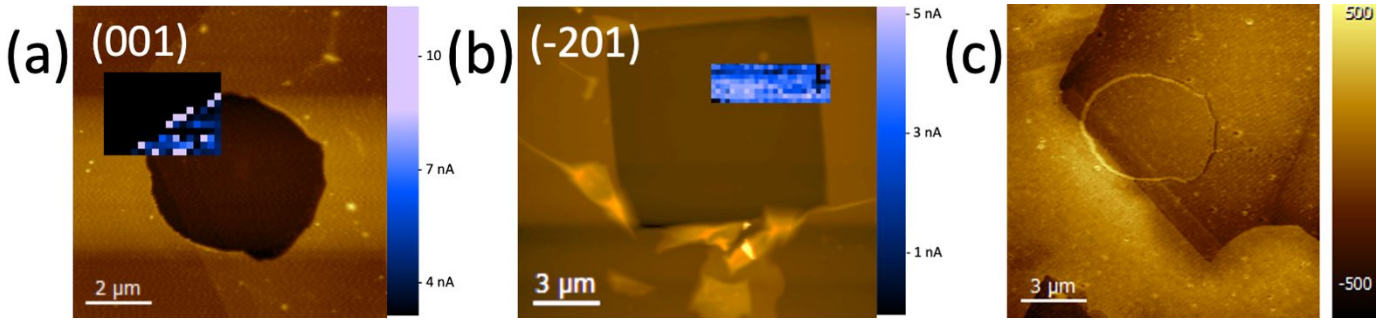

Fig. 5: C-AFM (a,b), magnitude and (c) mappings of two 2D/3D junctions formed on (-201)-oriented and (001)-oriented Ga_2O_3 substrates. Inset in (a) and (b) have units of nA. z-axis scale bar for KPFM images is millivolts (mV).

Orientation	Ideality		V_{on}	
	Center	Side	Average	Standard deviation
(-201)	3.42	8.57	2.12	0.069
(001)	77.38	276.67	3.96	1.18

Table 2 Ideality factor and turn-on voltage extracted from C-AFM measurements for WSe_2 flakes on two β-Ga_2O_3 orientations. We attribute the higher ideality values of the (001) orientation to accumulated damage of the probe tip and junction during measurement.

Conclusions

In conclusion, plenty of high-performing diode and p-n heterojunctions based on 2D/3D interfaces have been demonstrated in the past (Fig. 6). These have seldom explored β-Ga_2O_3 as a substrate material, opting for more well-established wide-bandgap semiconductors like GaN despite their lower breakdown voltages, smaller bandgaps and the low production costs of Ga_2O_3.[2,3,4] This is in part due to the uncertain effects of the semiconductor's proven anisotropy. Here, we have fabricated and investigated 2D/3D vertical diodes on β-Ga_2O_3 single-crystal substrates via stacking 2D crystals on 3D Ga2O3 and investigating their electrical transport. We found that these junctions are optimized for diode performance in planar orientation (-201) of the Ga_2O_3, 2D WS_2 as the other semiconductor and Ti/Au metal contacts to the 2D semiconductor. Their performance was also similar to recent reports on other 2D-based heterojunctions (Fig. 6). We verified the clean interfaces with transmission electron microscopy (TEM) cross-sections and measured the quality of our devices using AFM techniques, technology computer aided design (TCAD) simulations and high-temperature dependent I-V measurements. Our results suggest that the anisotropic properties of n-doped bulk β-Ga_2O_3 do in fact strongly influence device behavior, in the same fashion as the choice of contact metals and interfaced semiconductors. For WSe_2, we found that the lowest recorded ideality factor varies from 1.20 to 2.79 between different orientations of Ga_2O_3 substrate. This knowledge allows to predict relative Ga_2O_3-based heterojunction performance and consider how to better exploit this material's potential for future optoelectronic applications. Our findings demonstrate a facile fabrication of strongly rectifying and high ON current density heterojunctions and enable new avenues in Ga_2O_3 based solid state devices.

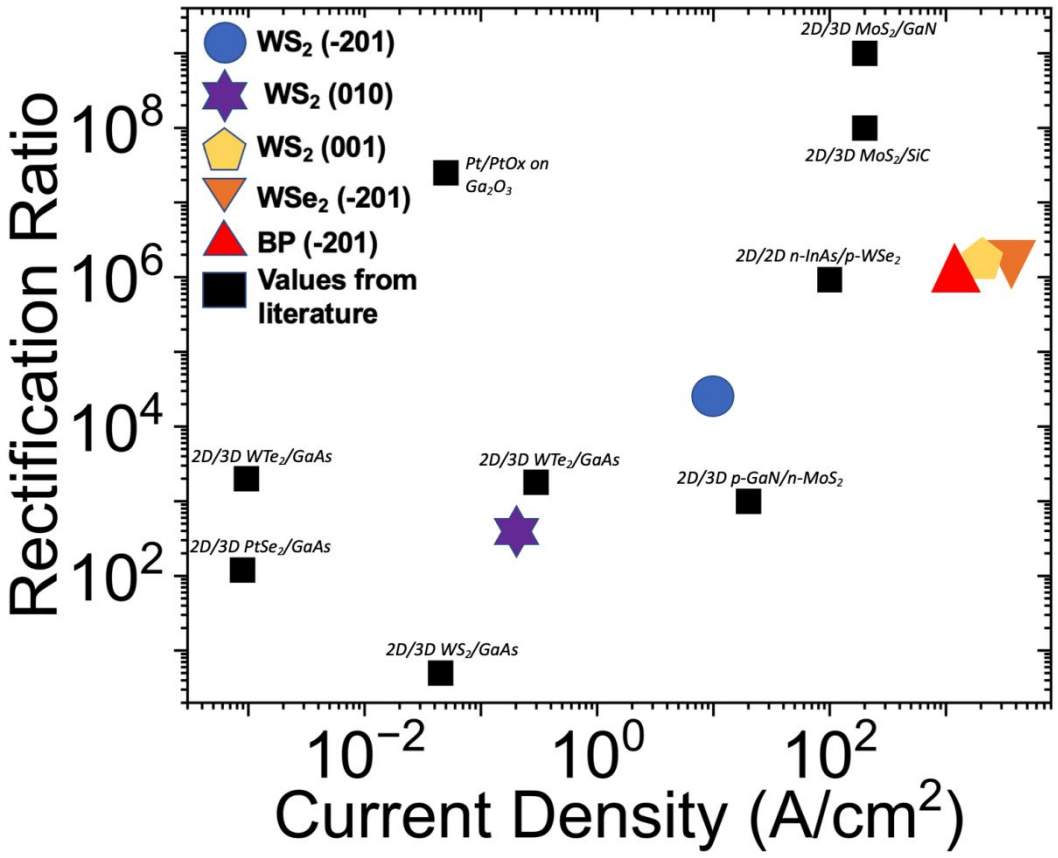

Fig. 6 Comparison of rectification ratios from the devices in Fig. 3 with values reported in the literature for diodes and p-n junctions[57,58,59,37,60,61,62,63,36]. The WS_2 (001), WSe_2 (-201) and BP (-201) ratios are among the lowest recorded for Ga_2O_3-based 2D/3D diodes.

Methods

Bulk β-Ga_2O_3 single crystals with varying crystallographic orientations were grown using high-quality edge-defined film-fed growth (EFG) method and acquired from Novel Crystal Technology, Inc. (Table S3)[64,65]. All three β-Ga_2O_3 single crystal substrates have comparably the same n-doping concentration of [Sn] = 5 x 10^{18} cm^{-3} performed by ion implantation. WSe_2 and WS_2 flakes were mechanically exfoliated from bulk crystals and transferred under ambient conditions. Because BP is highly sensitive to humidity, the transfer was performed in an argon environment with oxygen levels kept below 20 ppm. All three crystals were purchased from HQ Graphene and 2D Semiconductors. The electrodes and Al_2O_3 regions were patterned using an Elionix electron-beam lithography writer. The 2nm contact Al_2O_3 layer was electron-beam deposited onto the β-Ga_2O_3, which was degenerately n-doped with Sn. An additional ~38 nm was deposited using a Cambridge Nanotech S200 atomic layer deposition (ALD) system at 100°C. I-V measurements were carried out at room temperature with a linear voltage sweep of 0.05V incremental steps and a rate of approximately 2 V s^{-1} using a Keithley 4200A-SCS Parameter Analyzer. High-temperature measurements were performed with the same analyzer and with samples placed on a heating plate.

Contact metals were defined by electron-beam lithography patterning and e-beam evaporation. This method has been shown to yield low contact resistances in 2D devices such as BP-based FETs[66,28].

All junction simulations were implemented and performed in the SILVACO TCAD commercial software environment. Our knowledge of the physical models considered in this software allowed us to understand the physics at play in our experiments. Further details are provided in the supplementary materials.

A FEI Helios NanoLab 660 dual-beam microscope with focused ion beam scanning electron microscopy (FIB-SEM) was employed to prepare electron transparent cross-sectional samples. A FEI Titan 80-300 STEM/TEM equipped with a probe spherical-aberration corrector was employed to obtain HAADF-STEM and BF-STEM images with an operating voltage of 300 kV.

Acknowledgements

C.L. and D.J. acknowledge support for this work from the Air Force Office of Scientific Research (AFOSR) grant no. FA9550-21-1-0035. S.S acknowledges support for this work by Basic Science Research Program through the National Research Foundation of Korea (NRF) funded by the Ministry of Education (grant number 2021R1A6A3A14038492). This work was carried out in part at the Singh Center for Nanotechnology, which is supported by the NSF National Nanotechnology Coordinated Infrastructure Program under grant NNCI-2025608. H.Z. acknowledges support from the U.S. Department of Commerce, NIST under financial assistance award 70NANB22H101. A.V.D. acknowledges support from the Material Genome Initiative funding allocated to NIST. Disclaimer: Certain commercial equipment, instruments, software, or materials are identified in this paper in order to specify the experimental procedure adequately. Such identifications are not intended to imply recommendation or endorsement by NIST, nor it is intended to imply that the materials or equipment identified are necessarily the best available for the purpose. D.H.M. and H.F. acknowledges research supported as part of the ULTRA, an Energy Frontier Research Center funded by the U.S. Department of Energy (DOE), Office of Science, Basic Energy Sciences (BES), under Award # DE-SC0021230 and by the National Science Foundation (NSF) under Award # 2302696.

References

1 Huan, Y.-W. *et al.* Recent Advances in β-Ga2O3–Metal Contacts. *Nanoscale Research Letters* **13**, 1-10 (2018). https://doi.org:doi:10.1186/s11671-018-2667-2

2 Gong, H. *et al.* Band Alignment and Interface Recombination in NiO/B-Ga2O3 Type-II p-n Heterojunctions. *IEEE Transactions on Electron Devices* **67**, 3341 - 3347 (2020). https://doi.org:10.1109/TED.2020.3001249

3 Higashiwaki, M., Sasaki, K., Kuramata, A., Masui, T. & Yamakoshi, S. Gallium oxide (Ga2O3) metal-semiconductor field-effect transistors on single-crystal β-Ga2O3 (010) substrates. *Applied Physics Letters* **100** (2012). https://doi.org:10.1063/1.3674287

4 Mohamed, H. F. *et al.* Growth and fundamentals of bulk β-Ga2O3 single crystals. *Journal of Semiconductors* **40** (2019). https://doi.org:10.1088/1674-4926/40/1/011801

5 Wong, M. H., Sasaki, K., Kuramata, A., Yamakoshi, S. & Higashiwaki, M. Field-Plated Ga2O3 MOSFETs With a Breakdown Voltage of Over 750 V. *IEEE Electron Device Letters* **37**, 212-215 (2015). https://doi.org:10.1109/LED.2015.2512279

6 Cheah, L. B. *et al.* Ga2O3 thin films by sol-gel method its optical properties. *AIP Conference Proceedings* **2203** (2020). https://doi.org:10.1063/1.5142120

7 Siah, S. C. *et al.* Dopant activation in Sn-doped Ga2O3 investigated by X-ray absorption spectroscopy. *Applied Physics Letters* **107** (2015). https://doi.org:10.1063/1.4938123

8 Retamal, J. R. o. D., Periyanagounder, D., Ke, J.-J., Tsai, M.-L. & He, J.-H. Charge carrier injection and transport engineering in two-dimensional transition metal dichalcogenides. *Chemical Science* **9** (2018). https://doi.org:10.1039/c8sc02609b

9 Laturia, A., Put, M. L. V. d. & Vandenberge, W. G. Dielectric properties of hexagonal boron nitride and transition metal dichalcogenides: from monolayer to bulk. *2D Materials and Applications* **2** (2018). https://doi.org:10.1038/s41699-018-0050-x

10 Jo, S., Ubrig, N., Berger, H., Kuzmenko, A. B. & Morpurgo, A. F. Mono- and Bilayer WS2 Light-Emitting Transistors. *Nano Letters* **14**, 2019–2025 (2014). https://doi.org:10.1021/nl500171v

11 Shawkat, M. S. *et al.* Two-Dimensional/Three-Dimensional Schottky Junction Photovoltaic Devices Realized by the Direct CVD Growth of vdW 2D PtSe2 Layers on Silicon. *ACS Applied Material Interfaces* **11**, 27251–27258 (2019). https://doi.org:10.1021/acsami.9b09000

12 Irudayadass, G. & Shi, J. The estimation of impact ionization coefficients for beta-Ga2O3. (2018). https://doi.org:10.48550/arXiv.1806.01948

13 Guo, Z. *et al.* Anisotropic thermal conductivity in single crystal β-gallium oxide. *Applied Physics Letters* **106** (2015). https://doi.org:10.1063/1.4916078

14 Chen, H. *et al.* Characterizations of the nonlinear optical properties for (010) and (-201) beta-phase gallium oxide. *Optics Express* **26**, 3938-3946 (2018). https://doi.org:10.1364/OE.26.003938

15 Wong, M. H., Sasaki, K., Kuramata, A., Yamakoshi, S. & Higashiwaki, M. Electron channel mobility in silicon-doped Ga2O3 MOSFETs with a resistive buffer layer. *Japanese Journal of Applied Physics* **55** (2016). https://doi.org:10.7567/JJAP.55.1202B9

16 Schubert, M. *et al.* Anisotropy, phonon modes, and free charge carrier parameters in monoclinic $\ensuremath{\beta}$-gallium oxide single crystals. *Physical Review B* **93** (2016). https://doi.org:10.1103/PhysRevB.93.125209

17 Acar, M., Mobtakeri, S., Ertugrul, M. & Gur, E. Fabrication and Analysis Of 2D/3D Heterojunction Between Continuous Few-layer WS2 Film and Si (100). *Hittite J. Sci. Eng.* **8**, 01-05 (2021). https://doi.org:10.17350/HJSE19030000206

18 Pospischil, A., Furchi, M. M. & Mueller, T. Solar-energy conversion and light emission in an atomic monolayer p–n diode. *Nature Nanotechnology* **9**, 257-261 (2014). https://doi.org:10.1038/nnano.2014.14

19 Cui, Y. *et al.* High-Performance Monolayer WS2 Field-Effect Transistors on High-κ Dielectrics. *Advanced Materials* **27**, 5230-5234 (2015). https://doi.org:10.1002/adma.201502222

20 Cui, Y. *et al.* High-Performance Monolayer WS2 Field-Effect Transistors on High-κ Dielectrics - Cui - 2015 - Advanced Materials - Wiley Online Library. *Advanced Materials* **27**, 5230-5234 (2015). https://doi.org:10.1002/adma.201502222

21 Sheng, Y. *et al.* High-Performance WS2 Monolayer Light-Emitting Tunneling Devices Using 2D Materials Grown by Chemical Vapor Deposition. *ACS Nano* **13**, 4530-4537 (2019). https://doi.org:10.1021/acsnano.9b00211

22 Edmonds, M. T. *et al.* Creating a Stable Oxide at the Surface of Black Phosphorus. *ACS Applied Material Interfaces* **7**, 14557–14562 (2015). https://doi.org:10.1021/acsami.5b01297

23 Miao, J., Zhang, S., Cai, L. & Wang, C. Black Phosphorus Schottky Diodes: Channel Length Scaling and Application as Photodetectors. *Advanced Electronic Materials* **2** (2016). https://doi.org:10.1002/aelm.201500346

24 Miao, J. *et al.* Single Pixel Black Phosphorus Photodetector for Near-Infrared Imaging. *Small* **14** (2018). https://doi.org:10.1002/smll.201702082

25 Miao, J. *et al.* Air-Stable Humidity Sensor Using Few-Layer Black Phosphorus. *ACS Applied Material Interfaces* **9**, 10019−10026 (2017). https://doi.org:10.1021/acsami.7b01833

26 Jo, K. *et al.* Direct Optoelectronic Imaging of 2D Semiconductor–3D Metal Buried Interfaces. *ACS Nano* **15**, 5618–5630 (2021). https://doi.org:10.1021/acsnano.1c00708

27 Greiner, M. T., Chai, L., Helander, M. G., Tang, W.-M. & Lu, Z.-H. Metal/Metal-Oxide Interfaces: How Metal Contacts Affect the Work Function and Band Structure of MoO3. *Advanced Functional Materials* **23** (2012). https://doi.org:10.1002/adfm.201200993

28 Du, Y., Liu, H., Deng, Y. & Ye, P. D. Device Perspective for Black Phosphorus Field-Effect Transistors: Contact Resistance, Ambipolar Behavior, and Scaling. *ACS Nano* **8**, 10035–10042 (2014). https://doi.org:10.1021/nn502553m

29 Ito, H., Kaneko, K. & Fujita, S. Growth and Band Gap Control of Corundum-Structured α-(AlGa)2O3 Thin Films on Sapphire by Spray-Assisted Mist Chemical Vapor Deposition. *Japanese Journal of Applied Physics* **51** (2012). https://doi.org:10.1143/JJAP.51.100207

30 Pearton, S. J. *et al.* A review of Ga2O3 materials, processing, and devices. *Applied Physics Reviews* **5** (2018). https://doi.org:10.1063/1.5006941

31 Leroy, C. *Silicon Solid State Devices and Radiation Detection*. (World Scientific Publishing Co Pte Ltd, 2012).

32 Wei , Y. *et al.* Low Turn-On Voltage and High Breakdown Voltage β -Ga 2 O 3 Diode With Fin Channel and Ohmic Contact Anode. *IEEE Transactions on Electron Devices* **70**, 196-203 (2023).

33 Li, W. *et al.* in *2018 IEEE International Electron Devices Meeting (IEDM).* 8.5.1-8.5.4.

34 Wong, M. H., Murakami, H., Kumagai, Y. & Higashiwaki, M. Aperture-limited conduction and its possible mechanism in ion-implanted current aperture vertical β-Ga2O3 MOSFETs. *Applied Physics Letters* **118** (2021). https://doi.org:10.1063/5.0031561

35 Beeforth, T. H. & Goldsmid, H. J. *Physics of Solid State Devices*. (Pion, 1970).

36 Chuang, S. *et al.* Near-ideal electrical properties of InAs/WSe2 van der Waals heterojunction diodes. *Applied Physics Letters* **102** (2013). https://doi.org:10.1063/1.4809815

37 Kneiß, M. *et al.* Realization of highly rectifying Schottky barrier diodes and pn heterojunctions on κ-Ga2O3 by overcoming the conductivity anisotropy. *Journal of Applied Physics* **130** (2021). https://doi.org:10.1063/5.0056630

38 Miao, J. *et al.* Vertically Stacked and Self-Encapsulated van der Waals Heterojunction Diodes Using Two-Dimensional Layered Semiconductors. *ACS Nano* **11**, 10472–10479 (2017). https://doi.org:10.1021/acsnano.7b05755

39 Geller, S. Crystal Structure of β-Ga2O3. *Journal of Chemical Physics* **33** (1960). https://doi.org:10.1063/1.1731237

40 Ueda, N., Hosono, H., Waseda, R. & Kawazoe, H. Anisotropy of electrical and optical properties in β-Ga2O3 single crystals. *Applied Physics Letters* **71** (1997). https://doi.org:10.1063/1.119693

41 Ziman, J. M. *Electrons and Phonons: The Theory of Transport Phenomena in Solids*. (Oxford Classic Texts in the Physical Sciences, 2001).

42 Hogan, J. E., Kaun, S. W., Ahmadi, E., Oshima, Y. & Speck, J. S. Chlorine-based dry etching of B-Ga2O3. *Semiconductor Science and Technology* **31** (2016). https://doi.org:10.1088/0268-1242/31/6/065006

43 Jang, S. *et al.* A comparative study of wet etching and contacts on (-201) and (010) oriented B-Ga2O3. *Journal of Alloys and Compounds* **731**, 118-125 (2018).

44 Chen, M., Hack, J., Iyer, A., Lin, X. & Opila, R. L. in *Encyclopedia of Interfacial Chemistry* Vol. 4 (ed Klaus Wandelt) 547-552 (Elsevier, 2018).

45 Novoselov, K. S., Mishchenko, A., Carvalho, A. & Castro Neto, A. H. 2D materials and van der Waals heterostructures. *Science* **353** (2016). https://doi.org:10.1126/science.aac9439

46 Farmanbar, M. & Brocks, G. Controlling the Schottky barrier at MoS2/metal contacts by inserting a BN monolayer. *Physical Review B* **91** (2015).

47 Laturia, A., Van de Put, M. L. & Vandenberge, W. G. Dielectric properties of hexagonal boron nitride and transition metal dichalcogenides: from monolayer to bulk. *2D Materials and Applications* **2** (2018). https://doi.org:10.1038/s41699-018-0050-x

48 Polyakov, A. Y., Smirnov, N. B. & Shchemerov, I. V. Crystal orientation dependence of deep level spectra in proton irradiated bulk B-Ga2O3. *Journal of Applied Physics* **130** (2021). https://doi.org:10.1063/5.0058555

49 Ma, N. *et al.* Intrinsic Electron Mobility Limits in β-Ga2O3. *Applied Physics Letters* (2016).

50 Bulutay, C., Ridley, B. K. & Zakhleniuk, N. A. Polar optical phonon scattering and negative Kromer–Esaki– Tsu differential conductivity in bulk GaN. *Journal of Crystal Growth* **230**, 462–466 (2001).

51 Yu, Z. *et al.* Realization of Room-Temperature Phonon-Limited Carrier Transport in Monolayer MoS2 by Dielectric and Carrier Screening. **28**, 547–552 (2016). https://doi.org:10.1002/adma.201503033

52 Allain, A., Kang, J., Banerjee, K. & Kis, A. Electrical contacts to two-dimensional semiconductors. *Nature Materials* **14**, 1195-1205 (2015). https://doi.org:10.1038/nmat4452

53 Fu, H. *et al.* A Comparative Study on the Electrical Properties of Vertical (-201) and (010) B-Ga2O3 Schottky Barrier Diodes on EFG Single-Crystal Substrates. *IEEE Transactions on Electron Devices* **65**, 3507 - 3513 (2018). https://doi.org:10.1109/TED.2018.2841904

54 Ahmed, F., Choi, M. S., Liu, X. & Yoo, W. J. Carrier transport at the metal–MoS2 interface. *Nanoscale* **7**, 9222-9228 (2015). https://doi.org:10.1039/C5NR01044F

55 Ang, Y. S., Cao, L. & Ang, L. K. Physics of electron emission and injection in two-dimensional materials: Theory and simulation. *InfoMat* (2021). https://doi.org:10.1002/inf2.12168

56 Zhang, J. *et al.* Ultra-wide bandgap semiconductor Ga2O3 power diodes. *Nature Communications* **13** (2022). https://doi.org:10.1038/s41467-022-31664-y

57 Wang, J. *et al.* A Weyl semimetal WTe2/GaAs 2D/3D Schottky diode with high rectification ratio and unique photocurrent behavior. *Applied Physics Letters* **121** (2022). https://doi.org:10.1063/5.0109020

58 Zeng, L.-H. *et al.* Fast, Self-Driven, Air-Stable, and Broadband Photodetector Based on Vertically Aligned PtSe2/GaAs Heterojunction. *Advanced Functional Materials* **28** (2018). https://doi.org:10.1002/adfm.201705970

59 Jia, C. *et al.* An ultrasensitive self-driven broadband photodetector based on a 2D-WS2/GaAs type-II Zener heterojunction. *Nanoscale* **12**, 4435-4444 (2020). https://doi.org:10.1039/C9NR10348A

60 Lee, E. W. *et al.* Layer-transferred MoS2/GaN PN diodes. *Applied Physics Letters* **107** (2015). https://doi.org:10.1063/1.4930234

61 Giannazzo, F. *et al.* Highly Homogeneous 2D/3D Heterojunction Diodes by Pulsed Laser Deposition of MoS2 on Ion Implantation Doped 4H-SiC. *Advanced Materials Interfaces* **2201502** (2022). https://doi.org:10.1002/admi.202201502

62 Moun, M. & Singh, R. Exploring conduction mechanism and photoresponse in P-GaN/n-MoS2 heterojunction diode. *Journal of Applied Physics* **127** (2020). https://doi.org:10.1063/1.5143015

63 Yu, Y., Fong, P. W. K., Wang, S. & Surya, C. Fabrication of WS2/GaN p-n Junction by Wafer-Scale WS2 Thin Film Transfer. *Scientific Reports* **6** (2016). https://doi.org:10.1038/srep37833

64 Aida, H. *et al.* Growth of beta-Ga2O3 Single Crystals by the Edge-Defined, Film Fed Growth Method. *Japanese Journal of Applied Physics* **47** (2008). https://doi.org:10.1143/JJAP.47.8506

65 Higashiwaki, M. B-Ga2O3 material properties, growth technologies, and devices: a review. *AAPPS Bulletin* **32**, 1-14 (2022). https://doi.org:10.1007/s43673-021-00033-0

66 Ma, Y. *et al.* Black Phosphorus Field-Effect Transistors with Work Function Tunable Contacts. *ACS Nano* **11**, 7126–7133 (2017). https://doi.org:10.1021/acsnano.7b02858